Volume 3
Number 7
July 2022
Pages 797–984

RSC Chemical Biology

rsc.li/rsc-chembio

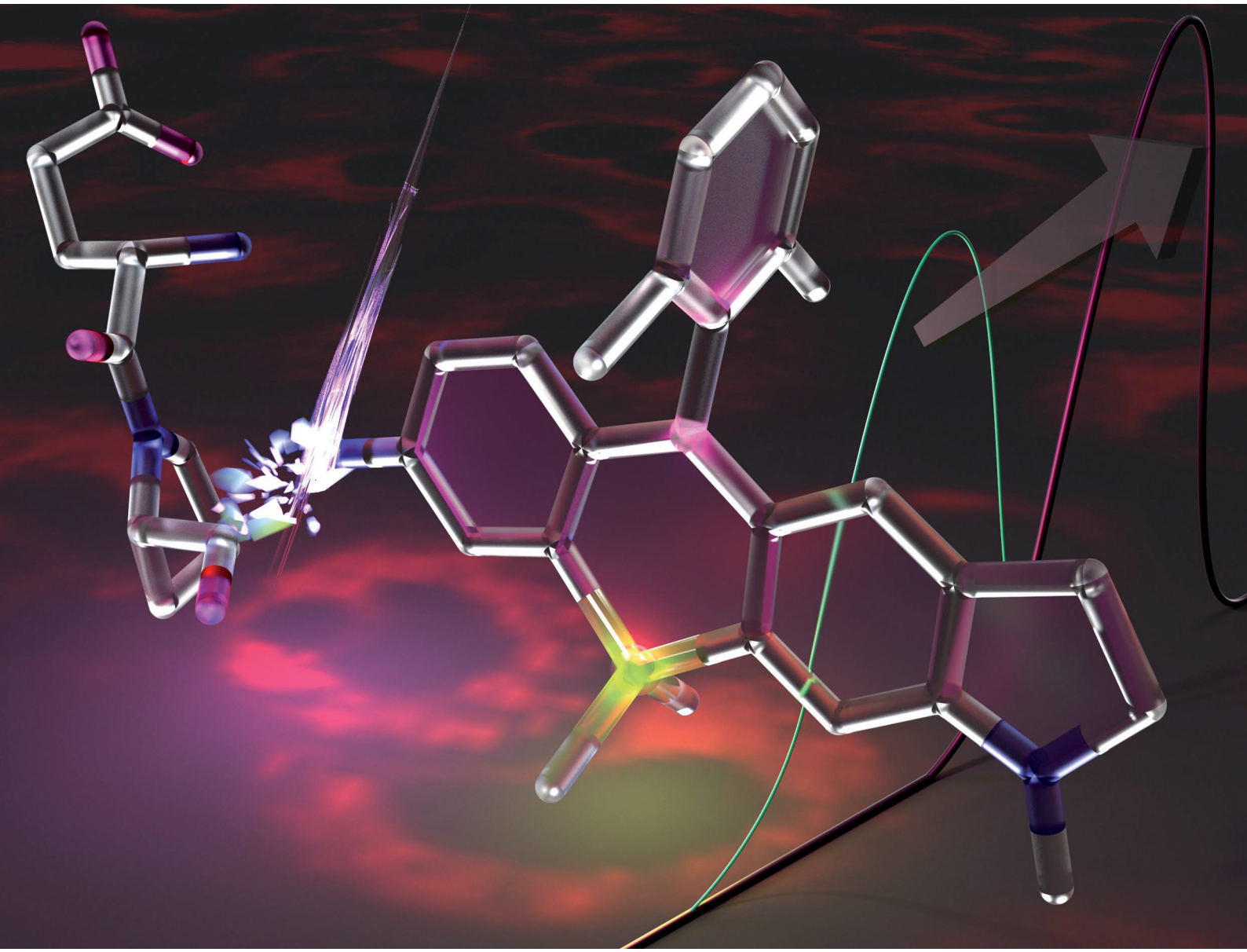

ISSN 2633-0679

ROYAL SOCIETY OF CHEMISTRY

PAPER

Kenjiro Hanaoka, Yasuteru Urano *et al.*
Molecular design of near-infrared (NIR) fluorescent probes targeting exopeptidase and application for detection of dipeptidyl peptidase 4 (DPP-4) activity

RSC Chemical Biology

ROYAL SOCIETY OF CHEMISTRY

PAPER

View Article Online
View Journal | View Issue

Cite this: *RSC Chem. Biol.*, 2022, 3, 859

Molecular design of near-infrared (NIR) fluorescent probes targeting exopeptidase and application for detection of dipeptidyl peptidase 4 (DPP-4) activity†

Yuki Hoshino,[a] Kenjiro Hanaoka,*[b] Kei Sakamoto,[c] Masahiro Yasunaga,[d] Takashi Kojima,[e] Daisuke Kotani,[e] Ayumu Nomoto,[a] Eita Sasaki,[b] Toru Komatsu,[a] Tasuku Ueno,[a] Hiroyuki Takamaru,[f] Yutaka Saito,[f] Yasuyuki Seto[c] and Yasuteru Urano*[ag]

Monitoring the activities of proteases *in vivo* is an important requirement in biological and medical research. Near-infrared (NIR) fluorescent probes are particularly useful for *in vivo* fluorescence imaging, due to the high penetration of NIR and the low autofluorescence in tissue for this wavelength region, but most current NIR fluorescent probes for proteases are targeted to endopeptidase. Here, we describe a new molecular design for NIR fluorescent probes that target exopeptidase by utilizing the >110 nm blueshift of unsymmetrical Si–rhodamines upon amidation of the N atom of their xanthene moiety. Based on this molecular design, we developed **Leu-SiR640** as a probe for leucine amino peptidase (LAP). **Leu-SiR640** shows a one order of magnitude larger fluorescence increment (669-fold) upon reaction with LAP than existing NIR fluorescent probes. We similarly designed and synthesized **EP-SiR640**, a NIR fluorescent probe that targets dipeptidyl peptidase 4 (DPP-4). We show that this probe can monitor DPP-4 activity not only in living cells but also in mouse organs and tumors. This probe could also detect esophageal cancer in human clinical specimens, based on the overexpression of DPP-4 activity.

Received 24th December 2021,
Accepted 2nd March 2022

DOI: 10.1039/d1cb00253h

rsc.li/rsc-chembio

Introduction

Proteases play important roles in a wide range of biological phenomena and their activities are deeply related to many diseases, including cancer and neurodegenerative, inflammatory and vascular diseases.[1–4] Proteases are also effective drug targets for the treatment of diseases such as hypertension (angiotensin-converting enzyme inhibitor),[5] HIV (HIV protease inhibitor),[6] and malignant melanoma (proteasome inhibitor).[7] Therefore, detecting the activities of proteases *in vivo* is important both in biological research to understand disease mechanisms and in medicine for clinical diagnosis.[8,9]

Activatable fluorescent probes are useful as chemical tools for detecting protease activities with high sensitivity and high temporal and spatial resolution.[10] Among them, near-infrared (NIR) fluorescent probes have recently attracted attention,[11] because NIR light (650–900 nm) shows high tissue penetration due to low absorption by biomolecules inside the body, and also because biological samples show low autofluorescence in this wavelength region.[12,13] Thus, NIR fluorescent probes enable the detection of the target protease activity even in the living body.

Many NIR fluorescent probes for detecting protease activities have been developed by conjugating NIR fluorescent dyes and dark quenchers such as BHQ3 and QSY21 *via* a protease-recognition peptide.[14,15] Their molecular design is based on the Förster resonance energy transfer (FRET) mechanism as a fluorescence-controlling off/on mechanism, and this approach

[a] *Graduate School of Pharmaceutical Sciences, The University of Tokyo, 7-3-1 Hongo, Bunkyo-ku, Tokyo 113-0033, Japan. E-mail: uranokun@m.u-tokyo.ac.jp*
[b] *Graduate School of Pharmaceutical Sciences, Keio University, 1-5-30 Shibakoen, Minato-ku, Tokyo 105-8512, Japan. E-mail: khanaoka@keio.jp*
[c] *Department of Gastrointestinal Surgery, Graduate School of Medicine, The University of Tokyo, 7-3-1 Hongo, Bunkyo-ku, Tokyo 113-8655, Japan*
[d] *Division of Developmental Therapeutics, Exploratory Oncology Research & Clinical Trial Center, National Cancer Center, 6-5-1 Kashiwanoha, Kashiwa, Chiba 277-8577, Japan*
[e] *Department of Gastroenterology and Gastrointestinal Oncology, National Cancer Center Hospital East, 6-5-1, Kashiwanoha, Kashiwa-shi, Chiba 277-8577, Japan*
[f] *Endoscopy Division, National Cancer Center Hospital, 5-1-1 Tsukiji, Chuo-ku, Tokyo 104-0045, Japan*
[g] *Graduate School of Medicine, The University of Tokyo, 7-3-1 Hongo, Bunkyo-ku, Tokyo 113-0033, Japan*

† Electronic supplementary information (ESI) available: Synthetic details, spectra, supporting figures, and experimental details. See https://doi.org/10.1039/d1cb00253h

can be applied to various NIR fluorophores. However, the molecular design can be applied only to probes for the enzymatic activity of endopeptidases that recognize a central region of the peptide sequence. In other words, these probes cannot detect the enzymatic activity of exopeptidases that recognize a terminal amino acid residue. Recently, a few NIR fluorescent probes for detecting exopeptidase activity have been developed by directly conjugating an amino acid to a NIR fluorophore.[16–18] However, these probes do not show a dramatic fluorescence increment when cleaved *via* the enzymatic reaction (less than 30-fold). Therefore, new approaches to the molecular design of NIR fluorescent probes for exopeptidase activity are still needed.

In recent years, we have established a synthetic scheme for a group of unsymmetrical Si–rhodamines, which are NIR fluorophores.[19] Rhodamines are widely used for fluorescence imaging because of their high fluorescence quantum yield, excellent photobleaching resistance, and high water solubility. In particular, unsymmetrical Si–rhodamines emit fluorescence in the far-red to NIR region, and it is possible to precisely control their absorption and emission wavelengths by means of alkyl substitution on the amino groups at the 3- and 6-positions of the xanthene ring. Here, we describe our discovery that unsymmetrical Si–rhodamine dyes showed very large blueshifts (>110 nm) of the absorption maximum when an amino group is converted to an amide group on the xanthene moiety. Although our previously reported symmetrical Si–rhodamine, SiR600, similarly showed a large blueshift, its fluorescence does not extend to the NIR wavelength region (~650 nm), and a longer fluorescence wavelength is needed for *in vivo* imaging.[20] Focusing on this photophysical property, we have developed a novel molecular design for NIR fluorescent probes that target exopeptidase activity. The developed probes show a fluorescence increase one order of magnitude higher than previously reported probes. As a proof of concept, we designed and synthesized **Leu-SiR640** as a NIR fluorescent probe for leucine aminopeptidase (LAP) activity. This probe showed a 669-fold fluorescent increase after the enzymatic reaction. We also developed **EP-SiR640** as a NIR fluorescent probe for dipeptidyl peptidase 4 (DPP-4) activity.

DPP-4 is a transmembrane exopeptidase that cleaves X-proline or X-alanine dipeptides from the peptide N-terminal. It hydrolyzes various biological peptides, including chemokines, neuropeptides, and bioactive peptides,[21,22] and is involved in various biological processes and diseases. For instance, glucose-dependent insulinotropic polypeptide (GIP) and glucagon-like peptide 1 (GLP-1), which are important for glucose homeostasis, are substrates of DPP-4, so DPP-4 inhibitors are widely used as therapeutic agents for type-2 diabetes.[23] In recent years, DPP-4 has also attracted attention as a drug target for cancer immunotherapy and many studies have confirmed its antitumor effect and examined the mechanism involved.[24–26] Furthermore, our group has found that fluorescent probes that target DPP-4 enable the rapid detection of esophageal cancer in resected tissue from patients,[27,28] and it has also been reported that DPP-4 is overexpressed in esophageal cancer by other researchers.[29] NIR fluorescent probes are expected to detect esophageal cancer in deeper regions compared with the previously reported green and red fluorescent probes for DPP-4. Therefore, we set out to develop a NIR fluorescent probe that targets DPP-4 activity, since we anticipated that this would be a powerful tool for studies of DPP-4-related biology and diseases, as well as a candidate for the clinical diagnosis of esophageal cancer. Indeed, **EP-SiR640** was able to detect DPP-4 activity in living cells and mice, as well as in tumor-bearing mice and specimens from esophageal cancer patients.

Results and discussion

Photophysical properties of unsymmetrical Si–rhodamines

First, we designed and synthesized three unsymmetrical Si–rhodamines that contain an amino group (**2,6-diMe SiR640**, **2,6-diMe JuloSiR**, and **2,6-diMe QuinoSiR**) as dye scaffolds for exopeptidase probes, as well as their acetylated derivatives (**Ac-2,6-diMe SiR640**, **Ac-2,6-diMe JuloSiR** and **Ac-2,6-diMe QuinoSiR**) (Fig. 1a). A 2,6-dimethylbenzene moiety was introduced into the probe structure to prevent the attack of bionucleophiles such as

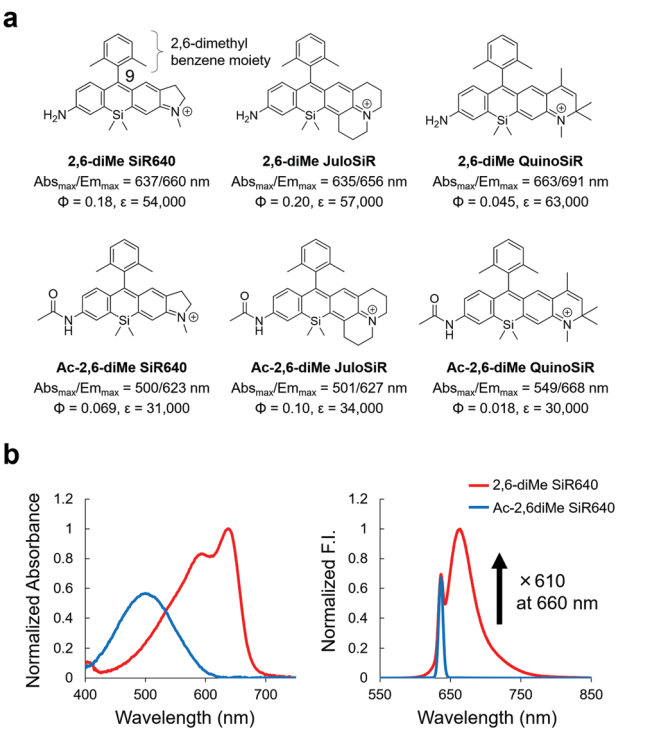

Fig. 1 Changes in photophysical properties upon amidation of unsymmetrical Si–rhodamines. (a) Chemical structures and photophysical properties in phosphate-buffered saline (PBS; pH = 7.4) of the synthesized unsymmetrical Si–rhodamines and their acylated derivatives. The fluorescence quantum yields were determined using a Hamamatsu Photonics Quantaurus-QY spectrometer, and the photophysical properties of **2,6-diMe SiR640** are taken from ref. 19. (b) Normalized absorption (left) and emission (right) spectra of 1 μM **2,6-diMe SiR640** and **Ac-2,6-diMe SiR640** in PBS (pH = 7.4) containing 0.1% DMSO as a co-solvent. The excitation wavelength was 637 nm. The sharp fluorescence peak of **Ac-2,6-diMe SiR640** is the Rayleigh scattering of the excitation light.

reduced glutathione (GSH) at the 9-position of the Si–xanthene moiety of each probe. Interestingly, all the unsymmetrical Si–rhodamines showed very large blueshifts (more than 110 nm) of the absorption maximum upon amidation of the amino group on the xanthene ring (Fig. 1b and Fig. S1, ESI†). Moreover, the molar extinction coefficients and the fluorescence quantum yields of these unsymmetrical Si–rhodamines were also reduced by the amidation (Fig. 1a).

Due to the changes in the photophysical properties, all the acetylated unsymmetrical Si–rhodamines showed almost no fluorescence when excited at the absorption maximum before acetylation. Therefore, all compounds having an amino group showed a more than 100-fold greater fluorescence intensity than their acetylated forms (Fig. 1b and Fig. S1, ESI†). Among them, **2,6-diMe SiR640** showed the largest fluorescence intensity change (610-fold). Furthermore, the absorption and fluorescence spectra of all these compounds did not change in the range of pH 3–10 (Fig. S2, ESI†). Based on these results, it was expected that **2,6-diMe SiR640** would be a good basic scaffold for highly sensitive NIR fluorescent probes that target exopeptidase activity.

To investigate in detail the mechanism of this large absorption spectral change, we investigated the molecular orbitals of the synthesized unsymmetrical Si–rhodamines using TD-DFT (time-dependent density-functional theory) calculations. As a result, the transition from S0 to S1 of all compounds was assigned as the transition from the HOMO to the LUMO (Fig. S3d, ESI†), and the decrease of the HOMO energy level of each compound was larger than that of the LUMO energy level after acetylation of the N atom on the xanthene ring (Fig. S3, ESI†). Thus, we consider that the HOMO–LUMO energy gap of each compound was increased by acetylation, resulting in the observed large blueshift of the absorption maximum.

We further examined whether or not this large blueshift is observed in solvents other than water. Interestingly, the blueshift of **Ac-2,6-diMe SiR640** in the absorption spectrum became larger (up to 123 nm) as the solvent polarity was increased, while **2,6-diMe SiR640** showed almost no blueshift regardless of the solvent polarity (Fig. S4, ESI†). Such fluorescent dyes that show a solvent polarity dependence of the absorption spectrum are known as environment-sensitive dyes. In general, the dipole moment of such dyes changes greatly between the ground state and the excited state, and is affected by the different degrees of solvent stabilization.[30] The large blueshift of the absorption maximum in a polar solvent, as observed in **Ac-2,6-diMe SiR640**, can be explained as negative solvatochromism.[31,32] Thus, it is considered that the acetylated unsymmetrical Si–rhodamines have a large dipole moment in the ground state, which is probably derived from the electron-withdrawing acetyl group, so that the blueshift of the absorption maximum in a polar solvent is larger than that in a less polar solvent (Fig. S5, ESI†). Thus, the large absorption wavelength difference between **2,6-diMe SiR640** and **Ac-2,6-diMe SiR640** probably arises because **2,6-diMe SiR640** is not environment-sensitive, like typical rhodamines, but becomes environment-sensitive after acetylation.

Design and synthesis of a NIR fluorescent probe for leucine aminopeptidase (LAP)

Next, we examined if **2,6-diMe SiR640** could be used as a scaffold for NIR fluorescent probes for exopeptidase activity. As a proof of concept, we designed and synthesized **Leu-SiR640** in which a recognition site for LAP, a leucine residue, was introduced into **2,6-diMe SiR640** (Fig. 2a), and we examined the absorption and fluorescence spectral changes after the enzymatic reaction. It was confirmed *via* HPLC analysis that the leucine residue of **Leu-SiR640** was cleaved by the enzymatic reaction with LAP to produce **2,6-diMe SiR640** (Fig. S6, ESI†). Concomitantly, we observed a large redshift of the absorption maximum (139 nm) and a large fluorescence increase (up to 670-fold) (Fig. 2a and b). This fluorescence increase was suppressed by a LAP inhibitor, bestatin (Fig. 2c). Furthermore,

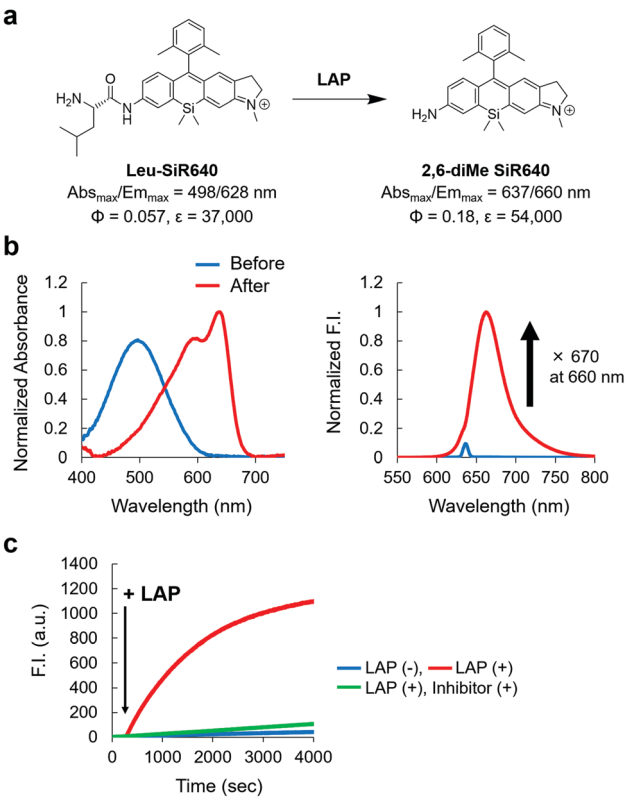

	V_{max} (M/sec)	K_m (μM)	k_{cat} (sec^{-1})	k_{cat}/K_m (M^{-1}·sec^{-1})
Leu-SiR640	7.82 × 10^{-9}	6.36	48.7	7.65 × 10^6

Fig. 2 NIR fluorescent probe for LAP activity based on the unsymmetrical Si–rhodamine scaffold. (a) The reaction scheme of **Leu-SiR640** with LAP and the photophysical properties. The data of **2,6-diMe SiR640** are taken from ref. 19. (b) Normalized absorption (left) and fluorescence (right) spectra of 1 μM **Leu-SiR640** upon addition of LAP (11 ng) in 10 mM HEPES buffer (pH = 7.4). The excitation wavelength was 637 nm. The sharp small fluorescence peak is the Rayleigh scattering of the excitation light. (c) Time course of the fluorescence intensity change of 1 μM **Leu-SiR640** upon addition of LAP (11 ng) at 300 s in 10 mM HEPES buffer (pH = 7.4). The excitation and emission wavelengths were 637 nm and 660 nm, respectively. The concentration of the LAP inhibitor, bestatin, was 100 μM. (d) Kinetic parameters of **Leu-SiR640** with LAP.

Leu-SiR640 had a two orders of magnitude lower K_m and a one order of magnitude higher k_{cat}/K_m compared with the fluorescent probe based on 7-amino-4-methylcoumarin (AMC) (K_m = 189 μM, $k_{cat}/K_m = 6.33 \times 10^5$ M^{-1} s^{-1}),[33] which is a widely used substrate for LAP (Fig. 2d). Furthermore, **Leu-SiR640** showed a lower K_m and a one order of magnitude higher fluorescence increase than existing NIR fluorescent probes for the activity of LAP (Fig. S7, ESI†). These results suggest that our molecular design for NIR fluorescent probes based on unsymmetrical Si–rhodamines is valid, and our scaffold is indeed suitable for developing NIR fluorescent probes with extremely high fluorescence activation in response to exopeptidase activity.

Design and synthesis of a NIR fluorescent probe for DPP-4

We next applied this molecular design to develop a NIR fluorescent probe for DPP-4 activity. The second proline from the N-terminal is essential for DPP-4 substrate recognition, and glycine–proline is a typical recognition sequence for DPP-4. So, we designed and synthesized **GP-SiR640**, **EP-SiR640**, **DP-SiR640** and **SP-SiR640** in which different DPP-4 recognition sequences were introduced into the **2,6-diMe SiR640** scaffold, and examined the changes of their photophysical properties upon enzymatic reaction with DPP-4. HPLC analysis indicated that all these probes afford **2,6-diMe SiR640** upon enzymatic reaction with DPP-4 (Fig. S8, ESI†), and showed a large redshift of the absorption maximum (about 140 nm) and a >200-fold fluorescence increase, similar to the probe for LAP activity (Fig. 3b and Fig. S9, ESI†). These fluorescence increases were suppressed by the DPP-4 inhibitor sitagliptin (Fig. 3c and Fig. S10, ESI†). Furthermore, the enzymatic reaction constants of each fluorescent probe were determined (Fig. 3d). The K_m and k_{cat}/K_m values of each fluorescent probe were almost the same as those of a fluorescent probe based on AMC, **GP-AMC** (K_m = 34 μM, $k_{cat}/K_m = 7.6 \times 10^5$ M^{-1} s^{-1}),[34] which is a widely used fluorescent substrate. It is interesting that the k_{cat}/K_m value of **DP-SiR640** is about one-third that of **EP-SiR640**, and the slight structural difference between these probes may affect their enzymatic recognition by DPP-4.

We then examined the selectivity of these probes for DPP-4 *versus* various other prolyl peptidases. There are many prolyl peptidases other than DPP-4 in the human body, and among them, DPP-8, DPP-9, and fibroblast active protein (FAP) are reported to release N-terminal proline dipeptides.[23,35] So, we measured the fluorescence increase when various prolyl peptidases were added to each probe solution (Fig. 4). All the fluorescent probes showed a large fluorescence increase upon addition of DPP-4. Interestingly, **EP-SiR640** and **DP-SiR640** showed almost no fluorescence increase upon addition of DPP-9, whereas **GP-SiR640** and **SP-SiR640** showed a relatively large fluorescence increase. All the probes showed essentially no fluorescence increase when prolyl peptidases other than DPP-4 and DPP-9 were added. Among the probes, **EP-SiR640** showed the highest selectivity and reactivity to DPP-4, and we thought that it would be suitable for the selective detection of DPP-4 activity in living samples. The structure at the active site is highly conserved among dipeptidyl peptidases, including DPP-4 and DPP-9. For example, the hydrogen bonds between

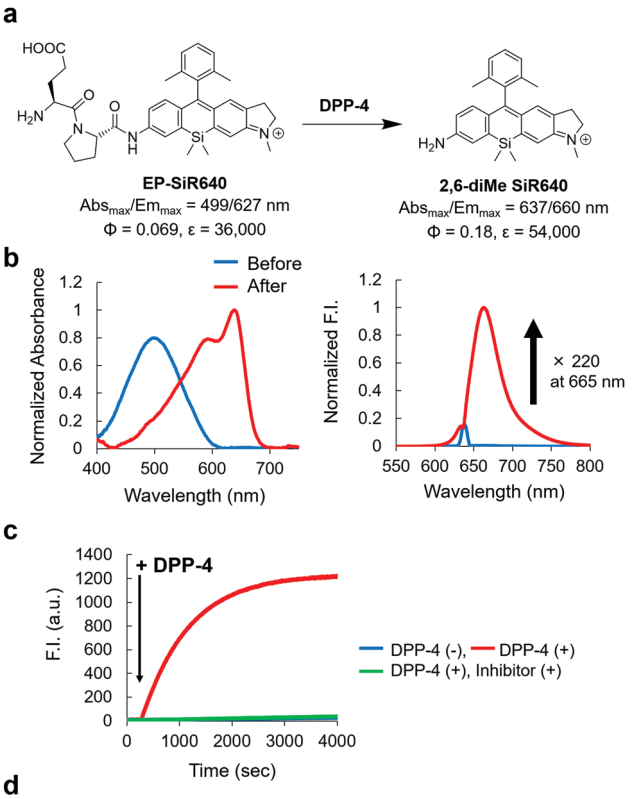

d

	V_{max} (M/sec)	K_m (μM)	k_{cat} (sec^{-1})	k_{cat}/K_m (M^{-1}·sec^{-1})
GP-SiR640	9.93×10^{-9}	26.5	8.76	3.31×10^5
EP-SiR640	7.10×10^{-9}	29.1	6.26	2.15×10^5
DP-SiR640	2.64×10^{-9}	36.2	2.33	6.44×10^4
SP-SiR640	6.69×10^{-9}	19.8	5.91	2.99×10^5

Fig. 3 NIR fluorescent probe for DPP-4 activity based on the unsymmetrical Si–rhodamine scaffold. (a) Reaction scheme of **EP-SiR640** with DPP-4 and the photophysical properties. The data of **2,6-diMe SiR640** are taken from ref. 19. (b) Normalized absorption (left) and fluorescence (right) spectra of 1 μM **EP-SiR640** upon addition of DPP-4 (0.24 μg) in 10 mM HEPES buffer (pH = 7.4). The excitation wavelength was 637 nm. The sharp small fluorescence peak is the Rayleigh scattering of the excitation light. (c) Time course of the fluorescence intensity change of 1 μM **EP-SiR640** upon addition of DPP-4 (0.24 μg) at 300 s in 10 mM HEPES buffer (pH = 7.4). The excitation and emission wavelengths were 637 nm and 660 nm, respectively. The concentration of the DPP-4 inhibitor, sitagliptin, was 1.8 μM. (d) Kinetic parameters of **GP-SiR640**, **EP-SiR640**, **DP-SiR640** and **SP-SiR640** with DPP-4.

the N-terminal amino group of the substrate peptide and Glu248 and Glu249 residues are essential for substrate recognition.[36] On the other hand, the active site of DPP-9 has a narrower space around the N-terminal amino acid residue of the substrate than that of DPP-4.[36] So, we assumed that **EP-SiR640** and **DP-SiR640** showed a low affinity for DPP-9 due to repulsion involving the negative charges of a carboxylic acid group of the probe and two glutamic acid residues at the active site of DPP-9.

Live-cell fluorescence imaging

We then applied **EP-SiR640** for live-cell fluorescence imaging of two different cell lines (H226 and KYSE270). First, the

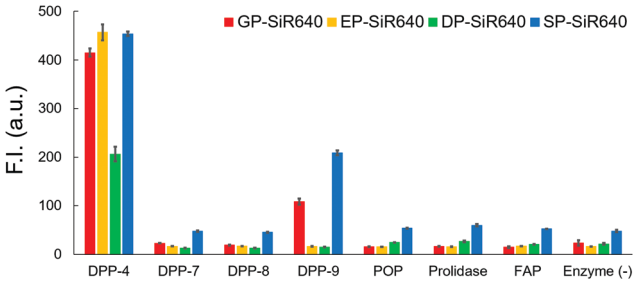

Fig. 4 Fluorescence intensity of 1 μM **GP-SiR640**, **EP-SiR640**, **DP-SiR640** and **SP-SiR640** upon addition of 0.1 μg mL^{-1} DPP-4 and related proteases in 10 mM HEPES buffer (pH = 7.4) containing 0.2% DMSO as a co-solvent. The excitation and emission wavelengths were 637 nm and 660 nm, respectively. Error bars represent ±S.E. (n = 4). POP, prolyl oligopeptidase; FAP, fibroblast activation protein.

expression of DPP-4 in both cells was confirmed *via* western blotting (Fig. S11, ESI†). Then, **EP-SiR640** was applied to both cell lines with or without the DPP-4 inhibitor (sitagliptin or K579). A fluorescence intensity increase of **EP-SiR640** was observed in both cell lines within 10 min after addition of the probe, and this fluorescence increase was significantly suppressed in the presence of the DPP-4 inhibitor (Fig. 5a and Fig. S12, ESI†). In addition, **EP-SiR640** was mainly localized in the mitochondria and partly in lysosomes and showed high intracellular retention, so that strong fluorescence was still observed even after three washing procedures (Fig. S13 and S14, ESI†). We also performed live-cell fluorescence imaging with four developed NIR fluorescent probes (**GP-SiR640**, **EP-SiR640**, **DP-SiR640** and **SP-SiR640**) to compare their fluorescence activation in living cells. These fluorescent probes were applied to H226 cells with or without the DPP-4 inhibitor. A fluorescence increase was observed with all the probes, and was suppressed in the presence of the DPP-4 inhibitor (Fig. 5b and Fig. S15, ESI†). Among them, **EP-SiR640** showed the largest fluorescence increase ratio after incubation for 60 min (Fig. 5c), in accordance with the *in vitro* experiments shown in Fig. 4. There are two possible reasons for this: (i) **EP-SiR640** shows high selectivity for DPP-4 among the various prolyl peptidases, as shown in Fig. 4; (ii) **EP-SiR640** shows lower membrane permeability than the other probes due to the negatively charged carboxylic acid group of the glutamic acid residue. DPP-4 is the membrane protein, and if the probe can easily enter the cells, an intracellular fluorescence increase would be observed independently of DPP-4 activity due to the enzymatic activation of the probe by intracellular enzymes other than DPP-4. The idea that **EP-SiR640** and **DP-SiR640**, which both have a carboxylic acid group, show low cell-membrane permeability is consistent with the observation that their fluorescence intensity in A549 cells, which have a low level of DPP-4 expression, is low compared to that of **GP-SiR640** (Fig. S16, ESI†).

Furthermore, we investigated whether or not **EP-SiR640** can detect differences of intracellular DPP-4 activity using various living cells. First, cell lysates of four different cell lines (H226, KYSE270, A549 and HEK293) were prepared, and the DPP-4 activity of each cell lysate was measured with **EP-SiR640**.

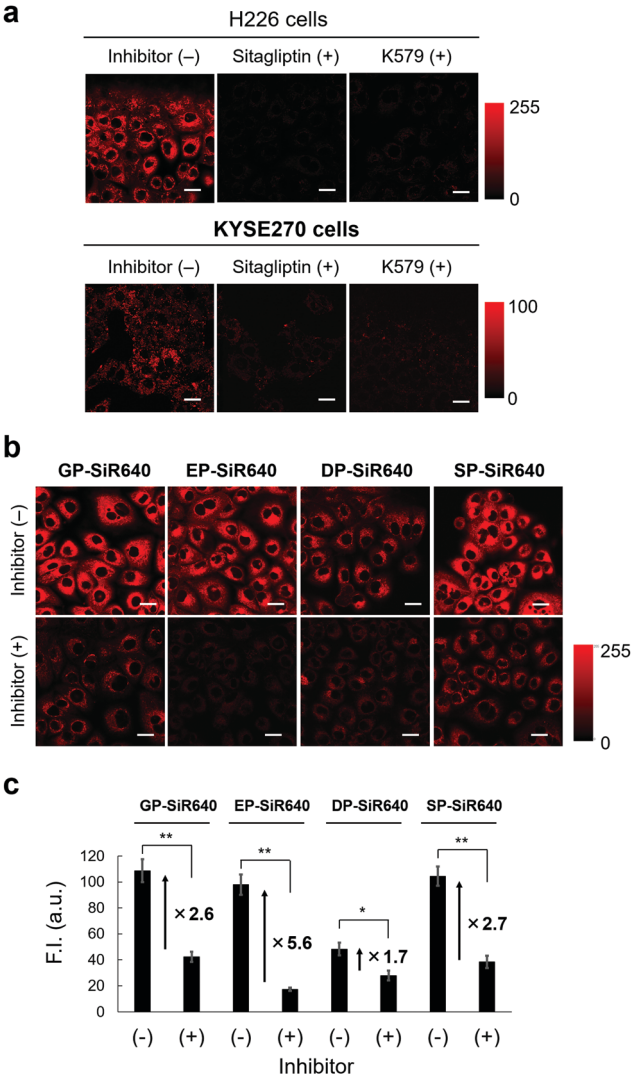

Fig. 5 Application of **GP-SiR640**, **EP-SiR640**, **DP-SiR640** and **SP-SiR640** for live-cell fluorescence imaging. (a) Fluorescence confocal microscopy images of live H226 and KYSE270 cells, which were incubated with or without the DPP-4 inhibitor (sitagliptin or K579). Each cell line was pre-incubated with 18 μM sitagliptin or 1 μM K579 for 30 min and then incubated with 1 μM **EP-SiR640** for 10 min. The excitation and emission wavelengths were 633 nm and 660–695 nm, respectively. Scale bars represent 25 μm. (b) Fluorescence confocal microscopy images of live H226 cells, which were incubated with or without the DPP-4 inhibitor (sitagliptin). Cells were pre-incubated with 18 μM sitagliptin for 30 min and then incubated with 1 μM **GP-SiR640**, **EP-SiR640**, **DP-SiR640** or **SP-SiR640** for 60 min. The excitation and emission wavelengths were 633 nm and 660–695 nm, respectively. Scale bars represent 25 μm. (c) Fluorescence intensities of H226 cells incubated with 1 μM each probe for 60 min. Error bars represent ±S.E. (n = 4); * and ** indicate $p < 0.05$ and $p < 0.01$ (Student's t-test), respectively.

Based on the fluorescence intensity increase of **EP-SiR640** in the cell lysates, it was confirmed that H226 and KYSE270 cells, which express DPP-4 as determined *via* western blotting (Fig. S11, ESI†), had a higher DPP-4 activity than A549 and HEK293 cells (Fig. S17a, ESI†). Then, fluorescence imaging of each cell line with **EP-SiR640** was performed. A fluorescence

increase was observed in H226 and KYSE270 cells, while no fluorescence increase was observed in A549 and HEK293 cells, in accordance with the cell lysate experiments (Fig. S17, ESI†). When we examined the expression of DPP-4 in A549 and HEK293 cells *via* western blotting, we observed the expression of DPP-4 in A549 and HEK293 cells as well as in H226 and KYSE270 cells (Fig. S11, ESI†). From the result, we think that the lower fluorescence intensity of A549 and HEK293 cells in the experiments with the cell lysate and the live-cell fluorescence imaging shown in Fig. S17 (ESI†) may be due to the low expression of the active form of DPP-4 in these cells. Thus, the enzymatic activity level of DPP-4 in the living cells could be monitored through fluorescence imaging with **EP-SiR640**.

In vivo fluorescence imaging

We next applied **EP-SiR640** to *in vivo* fluorescence imaging to examine whether or not this probe can detect endogenous DPP-4 activity in living mice. All animal procedures were approved by the Animal Care and Use Committee of the University of Tokyo. Saline or DPP-4 inhibitor (sitagliptin or linagliptin) in saline was orally administered to mice every day for one week, then **EP-SiR640** was intravenously administered, and fluorescence imaging was performed under anesthesia. Note that these two inhibitors are used in clinical practice to treat type-2 diabetes. We measured the time-dependent fluorescence increase of each exposed organ inside the body after the resection of the skin. When we performed the fluorescence imaging of mice orally administered with saline for a week after intravenous injection with 100 μM **EP-SiR640** *via* the tail vein, large and definite fluorescence increases were observed in the kidney, and the liver and the intestine, respectively (Fig. S18a, ESI†). So, it is considered that **EP-SiR640** was rapidly metabolized to **2,6-diMe SiR640** and excreted mainly *via* the kidney within an hour, while **2,6-diMe SiR640** had a high intracellular retention as shown in Fig. S14 (ESI†). On the other hand, the fluorescence intensity increase seen in living mice given saline was suppressed by the administration of DPP-4 inhibitor (Fig. S18, ESI†). In addition, after oral administration of saline or various concentrations of the DPP-4 inhibitor (sitagliptin or linagliptin) in saline to mice every day for 3 days, the mice were sacrificed and their organs were removed. Each organ was incubated with **EP-SiR640** aqueous solution, and *ex vivo* fluorescence imaging was performed. The fluorescence intensity increase was suppressed in a concentration-dependent manner by the DPP-4 inhibitors, and the DPP-4-inhibitory activity could be evaluated at the organ level (Fig. S19 and S20, ESI†). Both inhibitors inhibited the DPP-4 activity in all organs, especially the digestive organs such as the stomach and intestines, which may account for their therapeutic effect in type-2 diabetes. Linagliptin suppressed the DPP-4 activity in all organs at a lower dose (1 mg kg^{-1} day^{-1}) than sitagliptin, and this is consistent with the much lower dissociation constant (K_d) of linagliptin than that of sitagliptin.[37] Thus, this probe enables monitoring of the DPP-4 activity (not the biodistribution of the DPP-4 inhibitor) inside the body, with all the advantages of a fluorescent probe compared to a radioactive probe.

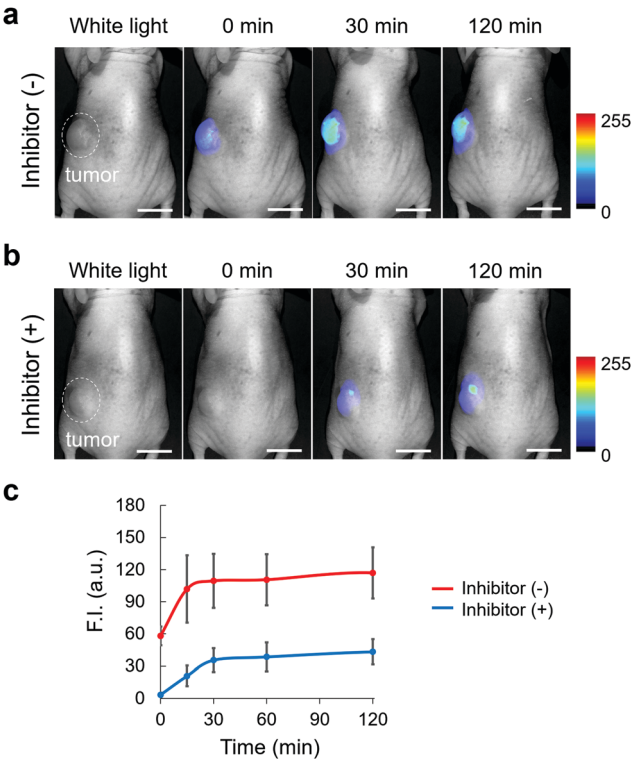

Fig. 6 Application of **EP-SiR640** for *in vivo* fluorescence imaging. (a and b) Fluorescence images of tumor-bearing BALB/cAJcl-*nu*/*nu* mice (female, 5 weeks old) intratumorally injected with saline or 0.05 mg sitagliptin in 10 μL saline, and then with 100 μM **EP-SiR640** in 10 μL saline containing 1% DMSO as a co-solvent. The excitation and emission wavelengths were 635 (616–661) nm and 700 nm, respectively. The scale bar represents 10 mm. (c) Fluorescence intensity change of the tumor. Error bars represent ±S.E. (n = 4).

Finally, we applied **EP-SiR640** to tumor imaging in mice and clinical specimens. First, we applied **EP-SiR640** to H226 tumor-bearing mice. Saline or DPP-4 inhibitor (sitagliptin) was intratumorally administered, and then **EP-SiR640** was also intratumorally administered. We observed a time-dependent increase of fluorescence in the tumor, and the fluorescence increase was suppressed in the presence of the DPP-4 inhibitor (Fig. 6 and Fig. S21, ESI†). Strong fluorescence was maintained even 2 hours after the administration of the fluorescent probe, suggesting that **EP-SiR640** is well retained in the tumors. The slight fluorescence observed in the tissues surrounding the tumor was considered to be due to leakage of the probe injected into the tumor or of the activated probe after enzymatic reaction in the tumor. Thus, **EP-SiR640** could fluorescently detect DPP-4 activity in the tumor *in vivo*.

Fluorescence imaging in clinical specimens

Next, we examined whether or not **EP-SiR640** could detect human esophageal tumors that express DPP-4. Our group has previously reported that green and red fluorescent probes that target DPP-4 are effective for detecting esophageal tumors in clinical specimens obtained *via* ESD (endoscopic submucosal dissection).[27,28] So, we examined if **EP-SiR640** could also detect

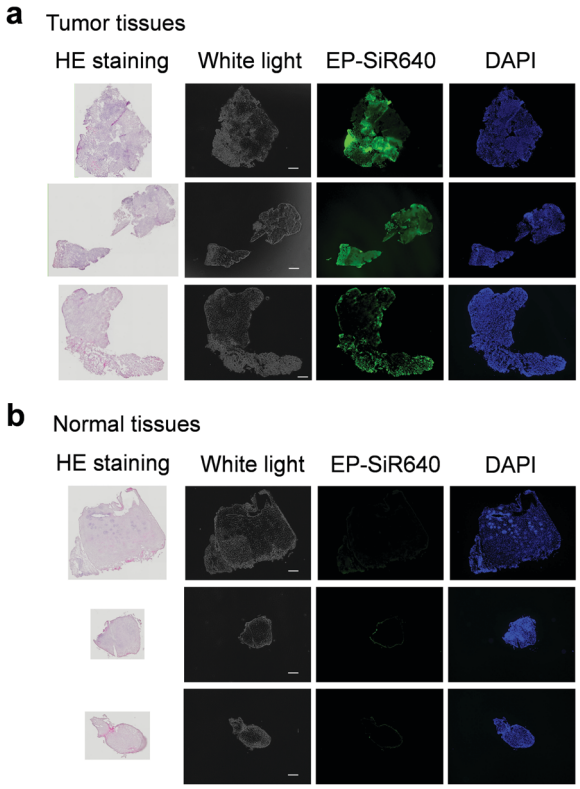

Fig. 7 Comparision of DPP-4 activity in esophageal cancer and normal tissues. (a and b) Fluorescence images of sections of human biopsy clinical specimens containing (a) esophageal cancer and (b) normal tissue. Each specimen was incubated for 50 min with 1 μM **EP-SiR640** and DAPI containing 0.1% DMSO as a co-solvent. The excitation and emission wavelengths were 620/60 and 700/75 nm for **EP-SiR640**, and 360/40 and 460/50 nm for DAPI, respectively. Scale bars represent 300 μm.

esophageal tumors in human ESD specimens. First, **EP-SiR640** was applied to sections of human biopsy clinical specimens containing esophageal tumor and normal tissues. All samples were confirmed to contain tumor or normal tissue through hematoxylin/eosin (HE) staining (Fig. 7). We observed strong fluorescence from the tumor tissues after the addition of **EP-SiR640**, while no such fluorescence increase was seen in normal tissues (Fig. 7). This result suggested that **EP-SiR640** can clearly distinguish between tumor and normal tissue sites in esophageal cancer biopsy specimens.

Finally, we applied **EP-SiR640** to the fluorescence imaging of esophageal tumor tissues in freshly resected ESD specimens. When **EP-SiR640** was applied to the esophageal tumor specimens, regions of squamous cell carcinoma (SCC) could be detected within 5 minutes based on the increased fluorescence (Fig. 8 and Fig. S22, ESI†). Furthermore, the boundary between the tumor and normal tissues was clearly demarcated, and was in good agreement with the boundary seen after Lugol staining and with the pathological diagnosis of the tumor. We further applied **EP-SiR640** to 6 ESD specimens of esophageal cancer. Although 2 small specimens showed a fluorescence increase in both normal and tumor regions, the others showed fluorescence images that coincided well with the Lugol staining

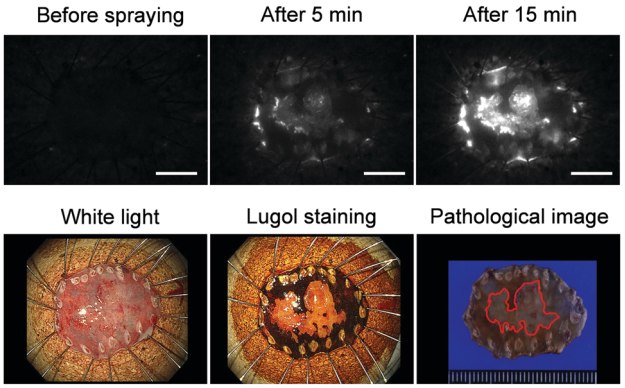

Fig. 8 Application of **EP-SiR640** to the detection of the esophageal cancer in freshly resected ESD tumor. Fluorescence images and white-light images before and after the Lugol staining, and a macroscopic pathological image of the esophageal tumor in the ESD specimen. 50 μM **EP-SiR640** in PBS (pH = 7.4) containing 0.5% DMSO as a co-solvent was added to the specimen. The excitation and emission wavelengths were 635 (616–661) nm and 700 nm, respectively. Scale bars represent 10 mm. The red line indicates the tumor lesion in the pathological image.

images (Fig. S23 and Table S1, ESI†). Thus, we succeeded in rapidly detecting esophageal tumors in freshly resected ESD specimens using **EP-SiR640**.

Conclusions

We have established a new molecular design strategy for NIR fluorescent probes that target exopeptidase activity and show a large fluorescence enhancement. This design is based on the large blueshift of unsymmetrical Si–rhodamines triggered by *N*-acetylation on their xanthene moiety. The synthesized unsymmetrical Si–rhodamines showed blueshifts of more than 110 nm upon acetylation of the N atom on the xanthene ring (Fig. 1a). We chose **2,6-diMe SiR640** as a scaffold, and developed **Leu-SiR640**, which showed a fluorescence increase of more than 600-fold upon enzymatic reaction with LAP, based on the large blueshift in the absorption spectrum of this scaffold. This fluorescence increase is an order of magnitude larger than that of existing NIR fluorescent probes for LAP activity. We also observed small fluorescence increases due to the non-enzymatic reaction in Fig. 2c and performed stability experiments for the synthesized probes (Fig. S24, ESI†). As a result, the stability of the probe was dependent on the cleaved group of the probe and further stabilization of the probe may be possible by designing the structure of the cleaved group. We believe our approach utilizing this unique blueshift of unsymmetrical Si–rhodamines provides a flexible platform for NIR fluorescent probes that target various exopeptidase activities. The large absorption change may also be useful for the detection of exopeptidase activity *via* photoacoustic imaging, which is a novel imaging modality that utilizes ultrasonic waves emitted after the photoexcitation of molecules.[38] Since ultrasonic waves have a higher tissue penetration than light,[38,39] these probes should be useful for the photoacoustic imaging of exopeptidase activity deep inside the body.

To demonstrate the usefulness of this molecular design strategy, we developed NIR fluorescent probes for detecting DPP-4 activity. By optimizing the DPP-4 recognition sequence, we succeeded in developing **EP-SiR640**, which detected DPP-4 activity in terms of a large fluorescence increase *in vitro* and was also applicable for the detection of DPP-4 activity in living cells. Furthermore, we could monitor the inhibitory activity of DPP-4 inhibitors towards endogenous DPP-4 inside the mouse body, as well as performing the *in vivo* fluorescence imaging of tumors in tumor-bearing mouse models. **EP-SiR640** generated strong fluorescence in tumor tissues, but not in normal tissues in human biopsy clinical specimens, as well as freshly resected ESD esophageal cancer specimens. An esophageal tumor could be detected within 5 min (Fig. 8). Since DPP-4 is involved in various biological phenomena and diseases, including cancer and type-2 diabetes, **EP-SiR640** is expected to be useful as a research tool for probing DPP-4-related biological phenomena and diseases, in addition to its clinical potential as a diagnostic aid.

Author contributions

Y. H. and K. H. planned the experiments and wrote the manuscript. Y. H., A. N. and E. S. synthesized compounds, measured photophysical data and performed fluorescence imaging of live cells and mouse models. K. S., Y. Seto, H. T. and Y. Saito performed the fluorescence imaging of ESD samples. M. Y., T. K. and D. K. performed the fluorescence imaging of biopsy samples. Y. H. and K. H. performed the TD-DFT study. K. H. and Y. U. planned the project. T. K. and T. U. advised on the experiments. All authors edited the manuscript.

Conflicts of interest

There are no conflicts to declare.

Acknowledgements

This work was supported in part by JSPS KAKENHI Grant Numbers JP20H02701, JP21H05262, JP20H04767, and JP18H04609, to K.H., JST SENTAN to K.H., Hoansha Foundation to K.H., Mochida Memorial Foundation for Medical and Pharmaceutical Research to K.H., Astellas Foundation for Research on Metabolic Disorders to K.H., The Tokyo Biochemical Research Foundation to K.H. and Nakatani Foundation for Advancement of Measuring Technologies in Biomedical Engineering to K.H. This work was also supported by AMED under Grant Number JP21ak0101182h0001 and JP21wm0325046s0101 to K.H. by a Grant-in-Aid for Scientific Research on Innovative Areas ''Singularity Biology (No. 8007)'' (JP19H05414 to K.H.) from The Ministry of Education, Culture, Sports, Science, and Technology, Japan.

References

1 M. Drag and G. S. Salvesen, *Nat. Rev. Drug Discovery*, 2010, **9**, 690–701.
2 M. Egeblad and Z. Werb, *Nat. Rev. Cancer*, 2002, **2**, 161–174.
3 J. Hu, P. E. Van den Steen, Q. X. A. Sang and G. Opdenakker, *Nat. Rev. Drug Discovery*, 2007, **6**, 480–498.
4 D. E. Bredesen, *Mol. Neurodegener.*, 2009, **4**, 27.
5 F. H. Messerli, S. Bangalore, C. Bavishi and S. F. Rimoldi, *J. Am. Coll. Cardiol.*, 2018, **71**, 1474–1482.
6 J. Mallolas, *AIDS Rev.*, 2017, **19**, 105–112.
7 S. Gandolfi, J. P. Laubach, T. Hideshima, D. Chauhan, K. C. Anderson and P. G. Richardson, *Cancer Metastasis Rev.*, 2017, **36**, 561–584.
8 P. Cheng and K. Pu, *Nat. Rev. Mater.*, 2021, **6**, 1095–1113.
9 Z. Zeng, S. S. Liew, X. Wei and K. Pu, *Angew. Chem., Int. Ed.*, 2021, **60**, 26454–26475.
10 H. W. Liu, L. Chen, C. Xu, Z. Li, H. Zhang, X. B. Zhang and W. Tan, *Chem. Soc. Rev.*, 2018, **47**, 7140–7180.
11 J. Bin, Li, H. W. Liu, T. Fu, R. Wang, X. B. Zhang and W. Tan, *Trends Chem.*, 2019, **1**, 224–234.
12 R. Weissleder, *Nat. Biotechnol.*, 2001, **19**, 316–317.
13 J. V. Frangioni, *Curr. Opin. Chem. Biol.*, 2003, **7**, 626–634.
14 T. Myochin, K. Hanaoka, T. Komatsu, T. Terai and T. Nagano, *J. Am. Chem. Soc.*, 2012, **134**, 13730–13737.
15 M. Verdoes, K. Oresic Bender, E. Segal, W. A. Van Der Linden, S. Syed, N. P. Withana, L. E. Sanman and M. Bogyo, *J. Am. Chem. Soc.*, 2013, **135**, 14726–14730.
16 X. He, L. Li, Y. Fang, W. Shi, X. Li and H. Ma, *Chem. Sci.*, 2017, **8**, 3479–3483.
17 W. Zhang, F. Liu, C. Zhang, J. G. Luo, J. Luo, W. Yu and L. Kong, *Anal. Chem.*, 2017, **89**, 12319–12326.
18 B. Wu, Y. Lin, B. Li, C. Zhan and S. Wu, *Anal. Chem.*, 2018, **90**, 9359–9365.
19 K. Hanaoka, Y. Kagami, W. Piao, T. Myochin, K. Numasawa, Y. Kuriki, T. Ikeno, T. Ueno, T. Komatsu, T. Terai, T. Nagano and Y. Urano, *Chem. Commun.*, 2018, **54**, 6939–6942.
20 Y. Kushida, K. Hanaoka, T. Komatsu, T. Terai, T. Ueno, K. Yoshida, M. Uchiyama and T. Nagano, *Bioorg. Med. Chem. Lett.*, 2012, **22**, 3908–3911.
21 E. E. Mulvihill and D. J. Drucker, *Endocr. Rev.*, 2014, **35**, 992–1019.
22 D. Röhrborn, N. Wronkowitz and J. Eckel, *Front. Immunol.*, 2015, **6**, 386.
23 D. Drucker, *Diabetes Care*, 2007, **30**, 1335–1343.
24 K. Ohnuma, R. Hatano and C. Morimoto, *Nat. Immunol.*, 2015, **16**, 791–792.
25 R. Barreira Da Silva, M. E. Laird, N. Yatim, L. Fiette, M. A. Ingersoll and M. L. Albert, *Nat. Immunol.*, 2015, **16**, 850–858.
26 A. Munitz and S. P. Hogan, *Nat. Immunol.*, 2019, **20**, 250–252.
27 H. Onoyama, M. Kamiya, Y. Kuriki, T. Komatsu, H. Abe, Y. Tsuji, K. Yagi, Y. Yamagata, S. Aikou, M. Nishida, K. Mori, H. Yamashita, M. Fujishiro, S. Nomura, N. Shimizu, M. Fukayama, K. Koike, Y. Urano and Y. Seto, *Sci. Rep.*, 2016, **6**, 26399.

28 A. Ogasawara, M. Kamiya, K. Sakamoto, Y. Kuriki, K. Fujita, T. Komatsu, T. Ueno, K. Hanaoka, H. Onoyama, H. Abe, Y. Tsuji, M. Fujishiro, K. Koike, M. Fukayama, Y. Seto and Y. Urano, *Bioconjugate Chem.*, 2019, **30**, 1055–1060.
29 K. Augoff, A. Hryniewicz-Jankowska, R. Tabola, L. Czapla, P. Szelachowski, J. Wierzbicki, K. Grabowski and A. F. Sikorski, *Oncol. Rep.*, 2014, **31**, 2820–2826.
30 A. S. Klymchenko and Y. Mely, *Prog. Mol. Biol. Transl. Sci.*, 2013, **113**, 35–58.
31 C. Reichardt, *Chem. Rev.*, 1994, **94**, 2319–2358.
32 P. Suppan, *J. Photochem. Photobiol., A*, 1990, **50**, 293–330.
33 R. E. Morty and J. Morehead, *J. Biol. Chem.*, 2002, **277**, 26057–26065.
34 M. Kawaguchi, T. Okabe, T. Terai, K. Hanaoka, H. Kojima, I. Minegishi and T. Nagano, *Chem. – Eur. J.*, 2010, **16**, 13479–13486.
35 J. S. Rosenblum and J. W. Kozarich, *Curr. Opin. Chem. Biol.*, 2003, **7**, 496–504.
36 B. Ross, S. Krapp, M. Augustin, R. Kierfersauer, M. Arciniega, R. Geiss-Friedlander and R. Huber, *Proc. Natl. Acad. Sci. U. S. A.*, 2018, **115**, E1437–E1445.
37 G. Schnapp, T. Klein, Y. Hoevels, R. A. Bakker and H. Nar, *J. Med. Chem.*, 2016, **59**, 7466–7477.
38 L. V. Wang and J. Yao, *Nat. Methods*, 2016, **13**, 627–638.
39 L. V. Wang and S. Hu, *Science*, 2012, **335**, 1458–1462.